HHS Public Access

Author manuscript

Biofabrication. Author manuscript; available in PMC 2019 January 16.

Published in final edited form as:

Biofabrication. ; 10(2): 025004. doi:10.1088/1758-5090/aa96de.

Automated fabrication of photopatterned gelatin hydrogels for organ-on-chips applications

Janna C. Nawroth[1,*,†], **Lisa L. Scudder**[1,*], **Ryan T. Halvorson**[1], **Jason Tresback**[2], **John P. Ferrier Jr.**[1], **Sean P. Sheehy**[1], **Alex Cho**[1], **Suraj Kannan**[1], **Ilona Sunyovszki**[1], **Josue A. Goss**[1], **Patrick H. Campbell**[1], and **Kevin Kit Parker**[1]

[1]Disease Biophysics Group, Wyss Institute for Biologically Inspired Engineering, John A. Paulson School of Engineering and Applied Sciences, Harvard University, Cambridge, MA, USA

[2]Center for Nanoscale Systems, Harvard University, Cambridge, MA, USA

Abstract

Organ-on-chip platforms aim to improve preclinical models for organ-level responses to novel drug compounds. Heart-on-a-chip assays in particular require tissue engineering techniques that rely on labor-intensive photolithographic fabrication or resolution-limited 3D printing of micropatterned substrates, which limits turnover and flexibility of prototyping. We present a rapid and automated method for large scale on-demand micropatterning of gelatin hydrogels for organ-on-chip applications using a novel biocompatible laser-etching approach. Fast and automated micropatterning is achieved via photosensitization of gelatin using riboflavin-5'phosphate followed by UV-laser-mediated photoablation of the gel surface in user-defined patterns only limited by the resolution of the 15-μm-wide laser focal point. Using this photopatterning approach, we generated microscale surface groove and pillar structures with feature dimensions on the order of 10 – 30 μm. The standard deviation of feature height was 0.3 μm, demonstrating robustness and reproducibility. Importantly, the UV-patterning process is non-destructive and does not alter gelatin micromechanical properties. Furthermore, as a quality control step, UV-patterned heart chip substrates were seeded with rat or human cardiac myocytes, and we verified that the resulting cardiac tissues achieved structural organization, contractile function, and long-term viability comparable to manually patterned gelatin substrates. Start-to-finish, UV-patterning shortened the time required to design and manufacture micropatterned gelatin substrates for heart-on-chip applications by up to 60 % compared to traditional lithography-based approaches, providing an important technological advance enroute to automated and continuous manufacturing of organ-on-chips.

Corresponding author: Kevin Kit Parker, Ph.D., Disease Biophysics Group, Wyss Institute for Biologically Inspired Engineering, John A. Paulson School of Engineering and Applied Sciences, Harvard University, 29 Oxford St, Pierce Hall 321, Cambridge MA 02138, kkparker@seas.harvard.edu.

[†]Current address: Emulate Inc., Boston, MA USA

[*]These authors contributed equally

Introduction

The ventricular myocardium of the human heart is composed of an anisotropic tissue structure that allows for force generation and contraction to pump blood throughout the body [1]. It has long been established that the collagen-rich, fibrous, extracellular matrix environment guides the formation of this laminar tissue architecture [2, 3]. The structural and mechanical properties of the cardiac microenvironment such as shape [1, 4], elastic modulus [5–7], and rigidity [8] alter cardiac calcium transient dynamics [4], electrophysiology [9], and contractile force generation [10–12]. The directed self-assembly of neonatal rat ventricular cardiac tissues into anisotropic sheets using microcontact printing techniques has been shown to enhance structural maturation, gene expression profile, and contractile function to levels comparable to those observed for adult rat myocardium [13]. This supports previous evidence that the extracellular matrix controls sarcomeric alignment and regulation of the actin cytoskeleton that is imperative toward improving the function of immature myocytes to a more adult phenotype [13–15]. Tissue engineering harnesses the ability to provide structural and mechanical input of the extracellular matrix to various cell types [11, 16, 17]. Organ-on-chip technology combines approaches from material science, cell biology, physiology, and tissue engineering with microsystems engineering and microfluidics to create a microphysiological environment of living cells that recapitulate human tissue and organ-level functions *in vitro* [18]. The goal of organs-on-chips is to improve preclinical assays for drug safety and development by mimicking the physiology and pathophysiology of healthy and diseased human tissues [18–23]. However, to become a next-generation tool for drug development and biomedical research in industry, organs-on-chips need to be amenable to large-scale continuous, automated, and quality-controlled fabrication, as opposed to the small-batch manufacture predominant in academic research. In particular, scalable fabrication strategies are needed for producing organ-specific 2D and 3D hydrogel extracellular matrix scaffolds that provide micromechanical cues for cellular adhesion, shape, differentiation, and cell-cell interactions [13, 24]. Cardiac and skeletal muscle organ-on-chip platforms exploit deformable hydrogel substrates with topographical micropatterns to achieve the physiological organization needed to test drug-induced toxicity [25], quantify tissue architecture, contractile function [11, 17], and human cardiovascular diseases [7, 20, 26].

Many approaches for micropatterning hydrogels have been developed and include stereolithographic “bottom-up” methods that pattern structures through layer-by-layer fabrication or molding. Alternatively"top-down” techniques involve the optical patterning of pre-formed hydrogels [27]. One of the most versatile and common “bottom-up” methods is the direct molding of patterned hydrogel surfaces and requires a sequence of interdependent photolithography and casting steps [5, 28, 29]. Current post-gelation optical patterning approaches can be done in a separate single step, but allow only for limited surface modifications [30]. Common to most of these patterning approaches is their limited scalability or ease-of-use, meaning that they do not simultaneously allow for high-throughput automation while supporting a wide range of possible pattern dimensions.

In this work, we propose a new photopatterning method for ablating and micropatterning gelatin hydrogels using an ultraviolet (UV) laser. Specifically, we adapted a UVA-light

activated photosensitizer (riboflavin-5'phosphate) and a UVA laser engraving system to photoablate the surface of uniform gelatin hydrogels and create anisotropic micropatterns suitable for tissue engineering and organ-on-chip applications. The novelty of the presented approach is that it enables maskless rapid micropatterning of a gelatin film without altering the hydrogel surface mechanics. The presented methods and results show that we have developed a novel tool for the automated and fast fabrication of micropatterned hydrogels for use in organ-on-chip applications.

In contrast to the currently wide-spread method of mechanical molding of gelatin, this approach allows for scalable fabrication strategies enroute to mass manufacture and standardization of organ-on-chip platforms. Specifically, our new top-down photopatterning method shortened the time needed to prototype gelatin substrates with a new pattern by 60% and enables the parallelization and temporal separation of more work steps compared to traditional photolithography-based bottom-up approaches using direct micromolding. As a quality control for our fabrication method, we validated the biocompatibility of UV-micropatterned gelatin for cardiac tissue engineering by quantifying the functional viability, contractile force, and sarcomeric structural orientation of neonatal rat and human iPS-derived cardiomyocytes (iPSCs). We also evaluated the ability to test novel patterns for single cell structural phenotyping of iPSCs. Finally, we tested this fabrication method as a rapid manufacturing process to produce engineered thin films used on our heart-on-a-chip platform and recapitulate appropriate contractile responses with neonatal rat cardiac tissues up to 27 days in culture [5, 31] .

Materials and Methods

Soft lithography fabrication of stamps for micromolding hydrogels

Elastomeric stamps were fabricated from polydimethylsiloxane (PDMS, Sylgard 184, Dow Corning, Midland, MI) using previously published protocols [29, 32]. In a cleanroom facility (Harvard Center for Nanoscale Systems), silicon wafers (Wafer World, West Palm Beach, FL) were rinsed, air dried, and plasma treated to clean the wafer and introduce polar groups to the surface. Next, wafers were coated with SU-8 3005 photoresist (MicroChem, Newton, MA) on a spin-coater (Spincoat G3P-8, Specialty Coating Systems, Inc., Indianapolis, IN) and spun at 4000 rpm to generate wafers with 5 μm feature height. Using forceps, wafers were transferred to a level 65°C hot plate for 30 seconds, then baked on a 95°C hot plate for 2 minutes. After cooling for 1 minute, customized photomasks with 10 μm lines separated by 10 μm-wide transparent lines were placed on top of the wafers, secured, and exposed to 355 nm wavelength UV light using a mask aligner system (ABM, Scotts Valley, CA). Following UV exposure, wafers were baked on hot plates at 65°C for 1 minute and 95°C for 1 minute. The wafers were then rinsed and developed in propylene glycol monomethyl ether acetate (Thermofisher Scientific, Waltham, MA) for up to 5 minutes to dissolve un-exposed regions. Next, wafers with surface patterns were dried and coated overnight with silane (United Chemical Technologies, Bristol, PA) in a vacuum chamber. PDMS was poured onto the wafers, cured at 65°C for at least six hours, carefully peeled from the wafer, and cut into stamps. These stamps featured 5 μm tall, 10 μm wide ridges spaced by 10 μm wide gaps that

were used for micromolding gelatin hydrogels with a line pattern. We compare the fabrication time of this method with UV laser micropatterning in Fig. 1.

Gelatin hydrogel fabrication

Several types of polymer slides (length × width ca. 75 mm × 25 mm) were tested as gelatin carriers, i.e., cyclic olefin copolymer (COC) Topas® 5013-S04 laboratory slides (0.27 mm thick, Polylinks, Arden, NC), cyclic olefin polymer (COP) Zeonor® 1420R laboratory slides (0.27mm thick, Polylinks), Clarex® PMMA (0.4 mm thick, Astra Products, Baldwin, NY), custom-cut polycarbonate (0.4 mm thick, McMaster-Carr), as well as the polyolefin Permanox® slides (ca. 0.25 mm thick, Thomas Fischer, Swedesboro, NJ) for these properties. Carrier slides were masked with low adhesive tape (orange tape, 3M, St. Paul, MN) to provide boundaries for the hydrogels. The masking tape was cut with an LPKF UV laser engraving system (355 nm wavelength, LPKF Laser and Electronics, Tualatin, OR) into 15 × 15 mm squares, for large tissues, or 18 mm diameter ellipses with an internal rectangular window for muscular thin film fabrication (Supplemental Fig. 1). The tape was removed to expose squares and inner rectangle for the heart-on-a-chip hydrogel substrates to plasma surface treatment. Carrier slides were oxygen plasma treated for 5 minutes using a Plasma Prep III reactor (Structure Probe, Inc. West Chester, PA) to clean and introduce polar groups to the surface of the slides to allow for strong adhesion of gelatin [33]. To prepare the gelatin hydrogel, 20% w/v type A porcine gelatin (175 g bloom, Sigma-Aldrich, St. Louis, MO) was dissolved in distilled water at 65°C. Cross-linking agent, 8% microbial transglutaminase (mTG) (Ajinomoto, Fort Lee, NJ) solution was warmed to 37 °C, degassed in a vacuum chamber for 2 minutes, and heated back to 37°C until fully dissolved. Equal parts of gelatin solution and mTG solution were mixed at a 1:1 ratio resulting in a final concentration of 10% w/v and 4% w/v, respectively. Note that this gelatin concentration generates a bulk elastic modulus of ca. 50–100 kPa, which supports physiological cardiomyocyte viability and function [5]. Lower concentrations of gelatin can mimic the native modulus of the heart (10–15 kPa) even more closely but these softer substrates tend to fracture during contractile assays and hence are not suitable for our application [5].

To cast the hydrogel substrates, 100–200 μl drops of the gelatin solution were pipetted onto each polymer carrier. MM gelatin hydrogels were fabricated as previously described [5], using the PDMS stamp described above, to mold a gelatin surface with 5 μm tall and 10 μm wide ridges separated by 10 μm wide gaps (i.e., 10 × 10 μm line patterns). For UV-M and unpatterned (UN) gels, a dry glass microscope slide cleaned with 70% ethanol was gently lowered onto the gelatin droplet until stopped by the bounding of the masking tape. The tape acted as a spacer for controlling gel thickness [5]. The gelatin was cured overnight for 12 hours in a humidified Petri dish. Once cured, the gelatin was hydrated with water to prevent adhesion to the glass and the glass slide was carefully peeled off the gelatin. For UV micropatterning, hydrated gelatin surface was treated with 0.05% (w/v) riboflavin-5’phosphate (Sigma-Aldrich) for 10 minutes. Following treatment, the gelatin gels were rinsed with water and immersed in distilled water for 10 minutes to remove excess riboflavin-5’phosphate. The slides were dried with filtered air for at least 30 minutes in a customized drying chamber on low speed. Once samples were completely dry, hydrogels were patterned with the UV laser engraver. For experiments detailed in Fig. 5, muscular thin

films (MTFs) were also cut out using the UV laser engraver at higher power settings. All samples were washed overnight in phosphate buffer solution (Thermofisher Scientific) to fully remove all riboflavin-5'phosphate from the gelatin. Remaining riboflavin is easily detected because it causes distinct yellow coloring of the gelatin. All solutions described were based in UltraPure DNAse/RNAse free distilled water (Thermofisher Scientific).

UV laser micropatterning and sample preparation

Designs for cell patterning were created in CorelDraw graphic design software (Corel Inc., Ottawa, Canada) and exported into CircuitCam and CircuitMaster software (LPKF Laser and Electronics), respectively. Prior to laser cutting, a micrometer was used to measure gelatin and polymer carrier slide thickness for calibration of the laser beam focus. The Protolaser U3 laser engraver with a 15-μm beam diameter was used to engrave the gelatin with vector lines spaced by 22 μm (as measured from beam center point) and to cut MTF cantilevers (2 mm × 1.3 mm) from the gelatin (Supplemental Fig. 1 and Supplemental Movie 1). For the generation of single cell islands, we employed the same spacing in the vertical and horizontal alignment to generate 7 μm × 7 μm (length × width) square micropillars. Laser beam speed, also referred to as mark speed, was adjusted such that the distance between untreated surface and line trough (i.e. half the wave amplitude) was greater than 2 μm, as measured using confocal microscopy (Zeiss Axio Observer, Oberkochen, Germany). The following laser settings produced micropatterned lines for UV-M and micropillar (μ-pillar) hydrogels: power = 0.13 to 0.16 Watts (W), frequency = 50 kilohertz (kHz), mark speed = 80 to 160 millimeters per second (mm/s), with 1 repetition. We used the following UV laser settings to cut through gels to produce MTF cantilevers: power = 0.3 W, frequency = 50 kHz, mark speed = 50 mm/s, with 20 to 50 repetitions. Mark speed and repetitions for cutting cantilevers were altered according to gelatin thickness and verified using stereoscope microscopy (Leica Microsystems, Inc., Wetzlar, Germany) and Nikon 500 digital camera (Nikon, Tokyo, Japan). The remaining gelatin was removed from the MTF cantilevers using forceps. Cantilevers were manually lifted off the carrier slide to fully detach from the polymer surface prior to cell seeding. All MM and UV-M substrates were disinfected with 70% ethanol for 5 minutes, rinsed with sterile phosphate buffer solution, and UV-sterilized under the UV light of a standard laminar flow hood for 5 minutes. Custom 8 mm tall rings made from Poly(methyl methacrylate), also known as PMMA, plexiglass or acrylic (McMaster-Carr, Robbinsville, NJ), were cut out with a laser engraving system (Epilog Laser, Golden, CO), disinfected with 70% ethanol for 5 minutes, dried with air, and UV-sterilized for 5 minutes in a UV ozone cleaner (Jelight Company, Inc, Irvine, CA). The rings were placed onto the gelatin-coated slides in a 6-well cell culture plate to direct cells onto the gelatin surface during seeding and prevent the slides from floating. All substrates were hydrated in sterile phosphate buffer solution until cell seeding. This method reduces the time required to prototype and manufacture micropatterned gelatin by up to 60% compared to traditional micromolding and soft lithography methods previous described (Fig. 1).

Fibronectin crosslinking of gelatin for human iPSC cellular attachment

For human iPS-derived cardiomyocyte (iPSC) experiments, we functionalized all gelatin hydrogel substrates (MM, UV-M, and plain) with covalently-bound fibronectin just before

seeding (Supplemental Fig. 2). This coating step is not required for rat neonatal cardiomyocyte culture, but we found that it greatly improves the viability and adhesion of iPSC on gelatin surfaces. A 0.1M sodium acetate buffer was prepared with sodium acetate (Sigma Aldrich) dissolved in deionized water and titrated with acetic acid and NaOH (Sigma Aldrich) until the pH reached 5.5. The sodium acetate buffer was then filtered in a sterile cell culture hood. We then dissolved 0.4 mg/ml 1-ethyl-3-(3-dimethylaminopropyl)carbodiimide hydrochloride (EDC, ThermoFisher Scientific) and 1.1 mg/ml sulfo-N-hydroxysuccinimide (NHS, Sigma) in fresh sodium acetate buffer in separate conical tubes. In the cell culture hood, EDC and NHS solutions were filtered with a 0.2 μm syringe filter for sterility. Next, 10 μl of EDC and 10 μl of NHS solutions were added to a 100 μl aliquot of sterile 1 mg/ml human fibronectin (BD Biosciences, San Jose, CA) and incubated for 15 minutes. After 15 minute incubation period, the entire EDC-NHS-fibronectin solution was diluted in sterile phosphate buffer solution for a final fibronectin concentration of 50 μg/ml and added to the surface of the gelatin hydrogels. Hydrogels were incubated in EDC-NHS-fibronectin solution for 2 hours at room temperature. Following incubation, gels were rinsed with fresh phosphate buffer solution three times and prepared for cell seeding. To verify the continuous coating of the gelatin surface with fibronectin, we immunostained the fibronectin (Supplemental Fig. 2A & B) using human fibronectin primary antibody (1:200, Sigma Aldrich) and following the protocols described in our methods section on immunostaining. We also show that the fibronectin staining is visible in the z-stack (bottom to surface of the gelatin) up to 12 μm (Supplemental Fig. 2B).

Atomic force microscopy imaging

Atomic force microscopy (AFM) imaging was performed using MFP-3D AFM system (Asylum Research, Santa Barbara, CA) with an open fluid droplet containing deionized water. The COC-gelatin slides were fixed to glass slides using carbon tape and sample bond adhesive (Ted Pella, Redding, CA) for mounting on the AFM stage. Prior to hydrogel contact, AFM cantilevers were calibrated in air and water using the Sader method to ensure reliable topography and elastic modulus measurements [34]. All topography images for hydrated hydrogels were collected in contact mode with soft, gold-coated silicon nitride bio-levers (Olympus TR400PB, Asylum Research Probe Store, Santa Barbara, CA) with a constant contact force ranging from 1 to 10 nN to prevent adhesion. After collecting a contact mode image of each gel sample in water, the tip was placed on three different sites on either the micropatterned ridges or troughs and at least 25 force distance curves (FDCs) were collected from each site. The scan rate (0.8 Hz) and distance traveled (1.5 μm) were kept constant for each FDC. All FDCs were analyzed using the Johnson-Kendall-Roberts (JKR) model [35] built into the instrument software to estimate the elastic modulus of the hydrogels.

Cell culture

Neonatal rat ventricular myocytes (NRVMs) were isolated from 2-day old neonatal Sprague-Dawley rats according to protocols approved by the Harvard University Animal Care and Use Committee. After isolation, ventricles were homogenized in Hanks balanced salt solution followed by overnight trypsinization and digestion with collagenase at 4°C (1 mg/mL, Worthington Biochemical Corp., Lakewood, NJ). Cell solutions were filtered and

re-suspended in M199 culture medium supplemented with 10% heat-inactivated fetal bovine serum (ThermoFisher Scientific), 10 mM HEPES, 0.1 mM MEM nonessential amino acids, 20 mM glucose, 2 mM L-glutamine, 1.5 mM vitamin B-12, and 50 U/mL penicillin (Sigma-Aldrich). Cells were pre-plated twice to reduce non-myocyte cell populations. Neonatal rat cardiac myocytes were seeded onto hydrogel substrates at a density of 2000 cells/mm^2. Cell culture medium was exchanged to maintenance medium containing 2% fetal bovine serum (FBS) every 48 hours [16].

For experiments with human iPS-derived cardiomyocytes (iPSCs, Axiogenesis, Cologne, Germany), cells were thawed from vials and plated in a 6-well culture dish in Cor.4U medium according to manufacturer's protocols. Two days prior to cell seeding onto UV-M line gels and micropillars (μ-pillars), cells were trypsinized with 0.25% trypsin-EDTA (ThermoFisher Scientific) for 5 minutes at 37°C and washed three times with warm Cor.4U medium. All cell culture medium was collected into a 15 ml conical tube and centrifuged at 200 × g for 5 minutes. The supernatant of the medium was aspirated to leave a pellet of human iPSCs. Cells were then re-suspended with 0.5 ml of Cor.4U medium and 20 μl of solution was removed for cell counting [5]. The tube of cells were kept at 37 °C while cell counting was performed using a standard hemocytometer. After cell counting, human iPSCs were dispersed onto line micropatterns at a seeding density of 2000 cells/mm^2 for tissues and a seeding density of 600 cells/mm^2 for single cell islands. Human iPS-derived cardiomyocytes were cultured for 9 days with media changes every 48 hours prior to fixation.

Immunostaining and structural analysis

Engineered cardiac tissues were pre-fixed with warm 2% paraformaldehyde (Electron Microscopy Sciences, Hatfield, PA) for 2 minutes, then fixed with fresh 4% paraformaldehyde and 0.05% Triton-X (Sigma-Aldrich) for 8 minutes. Tissues were gently washed three times with phosphate buffer solution and incubated with 5% (w/v) bovine serum albumin (BSA, Sigma-Aldrich) for 30 minutes. Next, tissues were then incubated with primary antibodies against sarcomeric α-actinin (1:200, Sigma-Aldrich), DAPI (1:200, Invitrogen, Carlsbad, CA) and Alexa Fluor 546 phalloidin (1:200, Invitrogen) for 60 minutes at room temperature. After the 60 minute incubation, tissues were gently rinsed three times for 5 minutes each with 0.5% BSA in phosphate buffer solution. Tissues were incubated with secondary antibodies against mouse IgG conjugated to Alexa Fluor 488 (1:200, Invitrogen) for 60 minutes. All antibodies described were diluted in 0.5% BSA and 200μl of solution was added to each tissue. Plates were covered with aluminum foil during incubation steps. Following incubation with secondary antibodies, tissues were gently rinsed three times with 0.5% BSA prior to mounting on glass slides. Stained hydrogels were mounted tissue side up on glass microscope slides and treated with Prolong Gold Anti-Fade reagent (Thermofisher Scientific). A 22 mm × 22 mm square glass slide was placed over the top of the hydrogel and left to dry overnight in a dark protected chamber prior to sealing the slide with nail polish. Slides were imaged using a Zeiss Axio Observer inverted confocal microscope (Zeiss) with 40x and 60x glycerol objectives. For each slide, multiple images with different fields of view were analyzed to determine the anisotropy and sarcomeric orientation of our engineered cardiac tissues and single cells. Custom algorithms

implemented in ImageJ and Matlab (The MathWorks Inc., Natick, MA) were used to compute the orientation angles of the lattice structure of sarcomeric α-actinin and the resultant vectors were used to calculate the total orientational order parameter (OOP). The OOP is defined as the mean resultant vector from the frequency distribution of α-actinin orientations that has been previously described by our laboratory and has been commonly used to describe liquid crystals [14, 36–38]. Here, the OOP is used for quantifying cardiac tissue alignment, where a value of 0 indicates an isotropic orientation and a value of 1 represent perfectly aligned sarcomeres [25].

The OOP is derived by (i) filtering and thresholding the sarcomeric α-actinin fluorescent image to extract the sarcomere edges as a binary signal, (ii) compute the structure tensor of the edges, (iii) extract the distributions of orientation angles from the structure tensor, and (iv) compute the OOP as the mean resultant vector from this angle distribution [14, 39]. The OOPs for each condition were averaged and statistically compared using Kruskal-Wallis one way ANOVA and Dunn's test or Student's t-test. To determine the orientation and packing density of sarcomeric α-actinin in single human iPSCs, we computed sarcomeric packing density (SPD) using custom ImageJ and Matlab (The MathWorks Inc.) algorithms as described previously [40]. The SPD used here is computed as the fraction of immunosignal that is localized in a regular lattice at the distance of the sarcomere. After extracting binary images of the sarcomeres as described for the OOP analysis above, the spatial frequencies describing the banded sarcomere patterns were identified using Fourier Transform. The presence and height of peaks in this frequency distribution is a direct measure of sarcomere lattice regularity [14]. Using a scoring system for maturation of the iPSC cytoskeleton, a score of 0 represents diffuse sarcomeric α-actinin staining and poor regularity of the sarcomere lattice, while a score of 1 represents a highly organized lattice of sarcomeric α-actinin. We then compared our SPD values with that of previously published results on microcontact-printed substrates [31].

Muscular thin film experiments and analysis

Muscular thin film (MTF) experiments were performed as previously described [5]. After 5 days in culture, heart chips were rinsed and immersed in a 60 mm Petri dish filled with warm Tyrode's solution (37°C) prior to video recording MTFs. The Tyrode's solution contained (mM): 135 NaCl, 1.8 $CaCl_2$, 5 KCl, 1.0 $MgCl_2$, 5 HEPES, 5 D-glucose, and 0.33 NaH_2PO_4 (Sigma-Aldrich). Next, cardiac tissues were imaged under a stereomicroscope (Model MZ6 with darkfield base, Leica Microsystems, Inc.) and all thin film cantilevers were peeled off the plastic carrier with forceps. To remove debris, tissues were transferred to a new 60 mm Petri dish with fresh Tyrode's solution at 37°C. A custom lid with platinum pacing electrodes was attached to the top of the Petri dish and connected to an electrical pulse generator (MyoPacer Cell Stimulator, IonOptix, Milton, MA) to deliver field stimulation at 1–2Hz and 5–10 V with a square wave pulse of 10 millisecond duration [6, 16]. Video recordings of both spontaneously contracting and paced MTF tissues were performed using a Basler area scan camera (100 frames per second, 1920 × 2000 pixels, Basler, Exton, PA) mounted to the stereomicroscope. Movies were imported into a customized tracking software, MTF Video Processor (MVP), to measure cantilever displacement. The MVP software performs frame-by-frame processing to subtract the

background, isolate the MTFs, detect the MTF edges, and use frame-by-frame subtraction to detect the edge displacement in *x*-projection as a function of time. The x-projections and corresponding time points of each movie were exported into a Microsoft Excel (.csv) file for further analysis. Given the *x*-projection data and original length of the cantilevers, the radius of curvature as a function of time was calculated for each MTF in Matlab [16]. The radius of curvature, thickness, and elastic modulus of each MTF were then used to calculate stress using a modified Stoney's equation [41].

The modified Stoney's equation is as follows: $\sigma = \frac{\mathrm{E}t_s^2}{6(1-v^2)Rt_c(1+\frac{t_c}{t_s})}$, where σ is the contractile stress exerted by the cardiac muscle layer, E is elastic modulus of the gelatin, t_s is gelatin thickness, R is MTF radius of curvature, t_c is the thickness of the cardiac muscle tissue, and υ is Poisson's ratio for an incompressible solid (0.5) [42]. Here, the elastic modulus was derived from the bulk stiffness modulus previously reported for gelatin hydrogels (55 kPa) [5]. As measured by confocal microscopy, gelatin film thickness was 180 μm, which is in agreement with previous studies [5]. Gelatin film thickness is determined by the thickness of the orange tape used in the fabrication process, as the tape serves as boundary and spacer for the gelatin cast onto the COC slides. Myocardium thickness was ~8 μm as measured using confocal microscopy. For each MTF, the average twitch stresses (difference between systolic and diastolic stress) for different pacing rates were calculated (Supplemental Table 1). Statistical significance was determined by Kruskal-Wallis one way ANOVA and Dunn's test using SigmaPlot software (Systat Software, San Jose, CA).

Results and Discussion

The myocardium in human and animal models is composed of an anisotropic tissue structure that allows for force generation and contraction [1]. Laminar cardiac tissues for organs-on-chips are typically engineered from isolated cells by micropatterning of the extracellular matrix and thereby mimicking the *in vivo* matrix architecture that provides anisotropic mechanical cues to the cells [25, 43, 44]. Previous work by our laboratory has shown that gelatin, which is derived from collagen, is an ideal substrate to generate organized, cardiac tissues for heart-on-a-chip applications and maintain cardiomyocytes in culture for long-term studies of cardiac contractile stress [5, 9].

In an effort to reduce processing time of manually molding gelatin for tissue engineering applications, we sought to identify top-down methods for batch processing patterned gelatin hydrogels by laser patterning gels for tissue alignment and producing 3-dimensional structures. Riboflavin-5'phosphate is used in clinical ophthalmology for collagen crosslinking (CXL) therapies for the treatment of keratoconus [45]. During CXL, the stroma of the eye is permeated with riboflavin-5'phosphate and exposed to low-intensity UVA radiation to stiffen the corneal collagen and increase corneal rigidity [46, 47]. The stiffening is thought to result from the UV-induced formation of singlet oxygen by riboflavin. These free radical species covalently join amino acid side chains in the collagen that cross-link neighboring collagen molecules leading to greater stiffness of the matrix [46, 48]. We reasoned that exposure of photosensitized gelatin to high-power UV laser light might also

allow for the localized absorption of light energy and allow for effective ablation of the gelatin surface for cardiac tissue engineering.

UV laser micropatterning of gelatin hydrogels

Here we sought to engineer micropatterned hydrogels for tissue engineering and organ-on-chip applications without the use of soft lithography or mechanical molding. For this, we initially developed a protocol for casting and adhering a thin gelatin film to a polymeric laboratory slide (Fig. 2A, blue square, and Fig. 2D). The objective was to identify a robust, biocompatible plastic carrier that would replace commonly used fragile glass slides [5], allow for controllable gelatin adhesion, and support optical imaging. We tested the cyclic olefin polymer (COP) Zeonor® 1420R, cyclic olefin copolymer (COC) Topas® 5013-S04 (both from Polylinks), Clarex® PMMA (Astra Products), polycarbonate (McMaster-Carr), as well as the polyolefin Permanox™ (Thomas Scientific) for these properties. We found that oxygen plasma treatment of COP, COC, and polyolefin carriers enabled robust adhesion of gelatin thin films [49–51], whereas gelatin was easily removable from non-treated carriers, or other polymer substrates, such as acrylic and polycarbonate (Supplemental Fig. 3). We then developed a method to micropattern the gelatin films with a UV laser engraving system (Supplemental Movie 1, Fig. 2B and 2E). Importantly, the 15 μm-wide UV beam diameter enabled us to design and generate patterns at scales similar to lithography-based micromolding (i.e. at the order of 1–20 μm) to mimic the anisotropic collagen-rich networks that guide cardiac tissue alignment in the ventricular myocardium [2, 52].

We discovered that UV-M parameters and consistency depended on the concentration of photosensitive agent, type of plastic carrier, and laser engraver speed. Regarding the first factor, it was essential to pre-treat the gelatin substrates with appropriate concentrations of photosensitive riboflavin 5’-phosphate (Fig. 2B and 2D). Optimal riboflavin pre-treatment concentration (0.05% w/v) allows for UV laser micropatterning of gelatin and generates uniform line patterns once laser parameters are calibrated (Fig. 2C and Supplemental Fig. 3A and B). Higher riboflavin concentrations require re-adjustment of the laser parameters to avoid burning, whereas omission of riboflavin treatment leads to formation of burn marks, bubbles and irregular surface patterns at all laser settings (Fig. 3F). We confirmed that for untreated gelatin hydrogels, the UV laser was only suitable for through-cuts. Second, it was essential to use a specific carrier composition. UV micropatterning of gelatin cast onto Zeonor®COP, Permanox™ polyolefin or polycarbonate resulted in partial micropatterning and occasional burning of the gelatin surface (Supplemental Fig. 3C and D). This is likely due to inherent differences in surface chemistry or optical properties between Zeonor®COP, Permanox™, and Topas® [49]. Conversely, PMMA also proved a suitable carrier for UV patterning (Supplemental Fig. 3E); however, the adhesion between gelatin and PMMA was very weak, leading to delamination upon rehydration of the gelatin. Third, the UV laser parameters for speed, power, and frequency were calibrated to achieve feature spacing, height, and width comparable to MM substrates for cardiac tissue engineering, as detailed in the methods. Thus, taking these factors into account, we developed a reliable protocol for UV micropatterning of gelatin hydrogels for use in tissue engineering and organ-on-chips applications.

Micromechanics of micromolded and UV laser micropatterned gelatin hydrogels

Our heart-on-a-chip platform aims to recapitulate the microenvironment of the human heart, including the low elastic modulus (<100 kPa) and laminar tissue structure [3, 16]. To test the flexibility and rapid prototyping capabilities of our UV laser micropatterning approach, we sought to engineer gelatin lines for cardiac tissue alignment and single-cell gelatin micropillars (μ-pillars, UV-μP) for human iPSC structural phenotyping. We also compared our method to traditional molding techniques by fabricating 10 μm by 10 μm PDMS stamps for micromolded (MM) gelatin to generate micropatterned gelatin lines (Fig 3A). We then used our UV-micropatterning fabrication approach described in Fig 2 to design and fabricate 15 μm by 7 μm spaced lines for UV-M gelatin (Fig 3B), and 7 μm by 7 μm spaced squares to create UV-μP gelatin islands (Fig 3C). To further investigate the biomechanics of hydrated UV-micropatterned gelatin compared to unpatterned (UN) and MM hydrogels, we used atomic force microscopy (AFM) to determine the topographical and elastic properties of the hydrogel surface for each condition [19].

Here we show that the grooves of MM gelatin hydrogels cast with PDMS stamps exhibit a square wave cross-section (Fig. 3D and Supplemental Fig 4A). By contrast, the grooves of UV-M gels exhibit a smoother, sigmoidal cross-section (Fig. 3E and Supplemental Fig 4B). Both UV-M hydrogels (mean height 3.9 ± 0.1 μm, n = 13, 4 samples) and MM hydrogels (3.4 ± 0.02 μm, n = 13, 4 samples) exhibit comparable feature heights within less than a micron from each other in peak to trough features (Fig. 3G and Supplemental Fig. 4A-B). The standard deviation of UV-M gelatin Z-sensor height is 0.3 μm, indicating that fabrication of these features are reproducible enough for large scale manufacturing of hydrogels for tissue engineering.

Atomic force microscopy also revealed that when UV-μP gels are hydrated, they expand to a 20 μm width from trough to trough (Fig. 3F) and exhibit a mean height of 2.6 ± 0.3 μm, (n = 3, 1 sample, Fig. 3G and Supplemental Fig. 4C). As a control we cast UN hydrogels onto COC slides and performed AFM topography measurements. From these measurements we discovered that the topography of UN gelatin does not vary by more than 150 nm over a 20 μm^2 area, ruling out substantial effects on the later UV-M topography (Supplemental Fig. 5).

In addition to measuring surface topography, we compared the elastic modulus of UN, MM, UV-M, and UV-μP gelatin using AFM force distance measurements in liquid to identify the impact of these micropatterning methods on substrate rigidity (Fig. 3H). All these gels contained 10% w/v gelatin and were crosslinked with 4% microbial transglutaminase; this composition is expected to result in a bulk elastic modulus of maximally 100 kPa, which is suitable for supporting physiological cardiomyocyte function but also provides sufficient stability for contractile assays [5]. To measure the actual elastic modulus of each substrate at their surface, we performed at least 25 force distance measurements at three independent sites and calculated the average elastic modulus using a Johnson-Kendall-Roberts model. Here, we only sampled at sites that would be in direct contact with cells. Specifically, on the line-patterned MM and UV-M substrates, we sampled the average elastic modulus both in top (crests) and bottom (troughs) locations whereas on UV-μP samples we only sampled from the raised pillars. We found that UN gelatin exhibits an elastic modulus of 33.2 ± 0.4 kPa (n = 88 force distance curves). MM hydrogels exhibit an elastic modulus of 107.3 ± 0.9

kPa (n = 131 force distance curves) which is consistent with previous results [53]. Interestingly, the MM elastic modulus is hence significantly higher than the elastic modulus of UN gels. This finding suggests that the mechanical casting of the patterns causes an increase in surface stiffness during curing, which might be due to surface stresses incurred during curing and shrinking at the interface of gelatin and mold [54]. Furthermore, UV-M hydrogels exhibit an average elastic modulus of 52.4 ± 0.7 kPa (n = 180 force distance curves), which is 30 kPa higher than the modulus of UN gels, yet 55 kPa lower than the modulus of MM gelatin. This suggests that with respect to surface stiffness, UV-M substrates are more similar to UN gelatin than are MM substrates. Finally, we measured the elastic modulus at the top of the UV patterned μ-pillars, where we anticipated cells to attach in subsequent experiments, to determine if patterning altered the surface modulus. AFM force distance measurements of UV-μP yielded an average modulus of 16.3 ± 1.1 kPa (n = 188 FDCs) which is lower than the elastic modulus of UN hydrogels and UV-M lines (not significant). This difference could result from the fact that the pillars are free to expand laterally in all directions, allowing a greater absorption of water by swelling which decreases the gel stiffness [55].

The surface elastic moduli are the upper boundary for the bulk elastic moduli in UV-patterned substrates. Although riboflavin-5'phosphate is allowed to fully penetrate the gelatin film during incubation, laser intensity will be attenuated with increasing penetration depth because riboflavin-5'phosphate strongly absorbs in the UV spectrum, and hence UV-mediated cross-linking is expected to be less pronounced beneath the surface.

In summary, the surface elastic modulus of UV micropatterned hydrogels is on the same order of magnitude as the elastic moduli of human and rat heart *in vivo* (10–15 kPa) [6, 56]. Moreover, UV-M and UV-μP hydrogels exhibit a smooth, sigmoidal surface topography with suitable dimensions for cardiac tissue engineering and single cell islands. Using this photopatterning approach, we generated microscale surface groove and pillar structures with maximum feature height variation of 0.3 μm, demonstrating robustness and reproducibility.

Cardiac tissue engineering of neonatal rat ventricular myocytes with UV laser micropatterning

Following the fabrication and mechanical characterization of UV micropatterned hydrogels, we set out to confirm that UV-M, like traditional MM substrates, will guide engineered tissue structure into recapitulating the anisotropic architecture of ventricular musculature on a 2-dimensional level. Therefore we seeded UV-M, MM, and UN gelatin substrates with neonatal rat ventricular cardiomyocytes (NRVMs) and investigated the expression and orientation of contractile proteins involved in myofibrillogenesis and contractile function [57].

Here we show that NRVMs seeded on UV-M substrates formed anisotropic monolayers similar to those observed for MM hydrogels (Fig. 4B and 4C). This is in stark contrast to NRVMs seeded on UN hydrogels (Fig. 4A). After 5 days in culture, we fixed and immunostained the NRVM tissues formed on our collagen-based hydrogels for sarcomeric α-actinin to investigate the expression and structural organization of contractile proteins (Fig. 4A-4C). Sarcomeric α-actinin is essential for stabilizing the contractile apparatus of

muscle tissues by localizing to the Z-disk of cardiomyocytes where it forms a lattice-like structure perpendicular to actin filaments [45]. Previous studies have shown that the orientation of sarcomeric α-actinin is representative of cardiomyocyte maturity and cardiac tissue alignment on our tissue constructs [9, 24, 46].

To quantify the degree of anisotropy, we computed the total orientational order parameter (OOP) of sarcomeric α-actinin from immunostained images. This parameter ranges from 0 (random organization) to 1 (perfect alignment) as a scoring system for cardiomyocyte tissue anisotropy [14, 36]. As expected, NRVM tissues engineered on plain gelatin surfaces (UN) formed isotropic monolayers of cells with an OOP of 0.04 ± 0.004 (n = 8 images, 3 slides). Cardiac tissues engineered on MM gelatin achieved a significantly higher OOP of 0.65 ± 0.01 compared to UN gels (n = 24 images, 3 slides), which is consistent with previous studies (Fig. 4H) [5, 29]. Interestingly, tissues on UV-M hydrogels reached an OOP of 0.85 ± 0.09 which is significantly higher than the OOP of both UN and MM hydrogels (n = 44 images, 4 slides), indicating a positive effect on sarcomere alignment and organization. Therefore, UV laser micropatterning of gelatin hydrogels is a sufficient and promising tool for tissue engineering applications where sarcomeric alignment is required.

To further validate the translation of our rapid manufacturing method to human cell models, we sought to engineer anisotropic cardiac tissues from human induced pluripotent stem cell-derived cardiomyocytes (iPSCs) on our UV-M hydrogels. We engineered MM and grooved UV-M substrates as previously described and seeded iPSCs onto these scaffolds as well as on UN substrates. On all substrates, the iPSCs form monolayers and express sarcomeric α-actinin but only tissues on patterned substrates show sarcomere alignment (Fig. 4D-4F). We quantified sarcomere alignment using OOP analysis that calculates the angles of orientation of cardiomycyte sarcomeres (Fig. 4G). MM tissues (n=14 images, 2 slides) achieve OOP values of 0.35±0.01. Showing almost identical alignment, UV-M tissue (n=20 images, 2 slides) reach OOP values of 0.34±0.01. As expected, tissues grown on UN gelatin (n=2 images, 1 slide) are isotropic and achieve significantly lower OOP values of 0.08±0.0054. Note that compared to NRVMs, the aligned human iPS cardiomyocytes reach distinctly lower OOP values. In general, we have found that human iPS cardiomyocytes, which tend to be immature and have a fetal phenotype [36], exhibit a lower average sarcomere alignment than rat neonatal cardiomyocytes.

Human iPSCs seeded on UV-M gelatin remain viable for more than one week in culture (fixed at 9 days) and exhibit spontaneous contractions along the UV micropatterns at ~1 beat per second (Supplemental Movie 2), which is comparable to tissues grown on MM micropatterns (Supplemental Movie 3).

To investigate cellular interactions with UV-μP single cell islands, we seeded iPSCs on these hydrogels and verified that cellular adhesion and sarcomeric α-actinin expression were in agreement with previous studies (Fig. 4I-J) [14]. Moreover, we found that human iPSCs responded to the μ-pillars in two distinct ways. In some cases, cells remained confined within the boundaries of a single pillar and assumed a spherical shape that we denoted as a ‘compact iPSC’ (Fig. 4I). Alternatively, ‘spread iPSCs’ expanded beyond a single pillar and aligned to one major axis, such that sarcomeric α-actinin is oriented around the nucleus of

the cell where the central pillar is located (Fig. 4J). We believe that these two morphologies are due to initial seeding conditions such as contact with neighboring cells and the position of the settling cell relative to neighboring pillars. We have not studied this effect further but it could be systematically explored by varying seeding density and the spacing of the pillars, for example.

We then investigated if human iPSCs seeded on UV-μP gels exhibited sarcomeric organization in agreement with previous microcontact printing studies [24]. Sarcomeric packing density (SPD) of contractile proteins, like α-actinin, are a metric of the degree of sarcomeric organization and cellular maturation of single iPSCs [24]. As detailed in the methods, the SPD is a scoring system for maturation of the iPSC cytoskeleton. A SPD score of 0 represents diffuse sarcomeric α-actinin staining and poor orientation, while a score of 1 represents a highly organized lattice of sarcomeric α-actinin. The SPD of human iPSCs seeded on our UV-μP gels exhibited an average of 0.22 ± 0.01 (1 slide, n = 8 images). This SPD value is in agreement with previously published experiments for human iPSCs seeded on microcontact printed islands where SPD is within a 0.1 to 0.3 range. This is typical of human iPSCs, as cellular maturation of the sarcomeric lattice structure is immature [31] and contain heterogeneous populations of myocytes [24]. Our results also suggest that in the future, UV laser micropatterning may aid in providing substrates for human iPSC single cell studies, including studies on 3-dimensional nuclear morphologies and cardiac contractile function of tissues [58], contractile force measurements of single cells using microposts [12, 59], and traction force microscopy techniques [60, 61].

Heart-on-a-chip applications of UV laser micropatterning

To further advance UV laser micropatterning as a rapid fabrication method for heart-on-a-chip applications, we applied this our new UV-laser patterning method to fabricate an established heart on-a-chip design called the muscular thin film (MTF) assay that enables the quantitative readout of contractile stress in engineered microtissues [17]. Heart-on-a-chip MTFs consist of engineered cardiac muscle tissue on micropatterned cantilevers [5]. This is achieved by measuring how far muscle contraction lifts up a thin polymeric or hydrogel cantilever, which provides a quantitative readout of contractile stress [16, 17, 62, 63]. As the muscle contracts, the cantilever bends, and the applied contractile stress can be computed from the cantilevers' curvature according to a modified Stoney's equation for deformation of stressed thin films [21, 25].

Here we investigated the contractile function of cardiac tissues engineered on UV-M hydrogels and developed a protocol to fabricate UV-M based MTFs (Supplemental Fig. 1). We then seeded NRVMs onto these constructs (Fig. 4C) to generate aligned cardiac tissues. The UV laser was employed for patterning the microgrooves and cutting out the thin film cantilevers simultaneously (Fig. 5A and Supplemental Fig. 1). Neonatal rat ventricular myocytes attached to the thin film cantilevers and exhibited spontaneous contractions in culture (Fig. 5Bi-ii, 5C, and Supplemental Movie 4). We used custom tracking software to measure the *x*-projection of the thin film cantilevers during spontaneous and electrically paced contractions (Fig. 5Bi-ii and Supplemental Movie 4, red bars). We then used these measurements to derive the films' curvature and corresponding contractile stress using a

modified Stoney's equation [17, 63] for diastolic (Fig. 5B i) and systolic states (Fig. 5B ii). We chose to use previously measured bulk stiffness of 55 kPa for these calculations as opposed to the surface stiffness of the gelatin, as this is more relevant to the cantilever movement through the medium [5, 21]. From the raw stress measurements (Fig. 5B iii), we subsequently quantified the difference between diastolic and systolic stress as the twitch stress (Fig. 5B iv, gray bars). During spontaneous contractions, UV-M MTFs exhibited average diastolic stresses of 24.7 ± 0.6 kPa and average systolic contractile stresses of 26.5 ± 0.7 kPa (n = 12 films); these values are on the same order of magnitude as previously published for MM MTFs [5]. With electrical pacing, diastolic stresses of UV-M MTFs remained at 23.4 ± 0.8 kPa at 1 Hz (n = 13 films) and 24.1 ± 0.7 kPa at 2 Hz (n = 9 films) (Fig. 4 iv and Supplemental Table 1). The systolic stress during pacing remained near-constant at 26.5 ± 1.0 kPa at 1 Hz and 27.3 ±1.2 kPa at 2 Hz. The average twitch stress increased non-significantly from 1.8 ± 0.3 kPa for spontaneously contracting thin films to 3.1 ± 0.4 kPa at 1 Hz and 3.3 ± 0.5 kPa at 2 Hz pacing (Supplemental Table 1). This result is in agreement with previous studies in MM hydrogels [5] and confirms that UV-M gels are suitable scaffolds for measuring cardiac contractile function. To this end, we have successfully fabricated UV-M hydrogels that support MTF technology without the need for soft lithography or mask design.

We then compared the spontaneous beat rate of engineered NRVM tissues on UV-M and MM gels over a 27 day period, as gelatin has been show in improved tissue viability and function for up to a month [5]. Here we show that NRVM tissues cultured on MM and UV-M gels exhibit similar beat rate patterns over the 27 day period (Fig. 5C). The beat rate for tissues cultured on MM gels from 1.5 ± 0.3 beats per second (day 3, n = 3 tissues) to 0.5 ± 0.1 beats per second (day 27, n = 3 tissues). The beat rate for tissues cultured on UV-M gels ranged from 1.2 ± 0.3 beats per second (day 3, 5 films) to 0.7 ± 0.5 beats per second (day 27, n = 3 films).

We then investigated the effect to long term culture on MTF contractile stress for UV-M tissues (Fig. 5D). Tissues cultured on UV-M MTFs were paced at 1 and 2 Hz as previously described. Long term culture significantly reduced diastolic stress to 12.6 ± 0.6 kPa at 1 Hz and 21.8 ± 0.01 kPa at 2 Hz (n = 2–3 films, 1 chip) compared to UV-M MTFs at 5 days in culture. Furthermore, UV-M MTFs cultured for 27 days exhibited systolic stresses comparable to tissues cultured for 5 days with mean systolic stress of 23.2 ± 0.1 kPa at 2 Hz and significantly reduced systolic stress of 17.7 ± 0.8 kPa at 1 Hz compared to tissues at 5 days at the same pacing rate (n = 2–3 films, 1 chip, Fig. 5Biv and 5D). Interestingly, long term culture did not significantly alter the contractile twitch stresses at 1 or 2 Hz with mean stresses of 5.1 ± 0.6 kPa and 1.5 ± 0.2 kPa, respectively (n = 2–3 films, 1 chip, Supplemental Table 1). This suggests that UV-M gelatin allows for the long term use of NRVM muscular thin films that can be adapted for more advanced heart-on-a-chip technologies.

In summary, our results show that our fabrication method of UV laser-mediated micropatterning of gelatin hydrogels allows for structural organization of sarcomeric α-actinin that is required to generate appropriate contractile responses on tissue-engineered muscular thin films. Furthermore, we demonstrate the ability to culture muscular thin films on our UV-M gels for a 27 day period, which makes them suitable for long-term studies on

this platform. These results serve as our quality control metrics for effective cardiac tissue engineering that can be adapted to microfluidic heart-on-a-chip technologies in future studies.

Conclusion and Outlook

Here, we presented a new UV-laser mediated photopatterning method for the automated and flexible top-down micropatterning of gelatin hydrogel films for tissue engineering application. Our approach complements the current methods for patterning hydrogel substrates using stamps [5] or 3D-printing [64], which are reliable and accurate techniques allowing for complex feature generation, but they are also costly, labor-intensive, and inflexible. In particular, we developed a protocol for activating gelatin hydrogels with a non-toxic UV-photosensitizer, riboflavin-5'phosphate, which allowed for the subsequent photoablation of micropatterns into the surface using a UV laser engraver. We identified and optimized three key parameters of reliable pattern generation including the type and concentrations of gelatin photosensitizers, UV laser parameters, and choice of carrier substrate. Using this method, we were able to design and fabricate standard micropatterned substrates for cardiac tissue engineering more than two times faster, but at the same microscale spatial resolution and low variability, compared to traditional, manual bottom-up fabrication using photolithography and micromolding. Importantly, our photopatterning method does not modify the stiffness of the gelatin surface. In contrast, we found that traditional micromolding of gelatin leads to a slight stiffening of the gel's surface compared to flat, homogeneous substrates, potentially by introducing stiffness-altering tensions during the cooling, drying and polymerization of the gelatin in the mold [54]. Hence, UV-patterning facilitates greater control of substrate stiffness, a major factor affecting cultured cell and tissue biology [65]. We further validated the suitability of UV-patterned substrates for cardiac muscle engineering using both primary neonatal rat cardiomyocytes and human induced pluripotent stem cell (iPSC) – derived cardiomyocytes. We show that, comparable to established MM substrates, the UV-M substrates support adhesion, alignment, contractile response, multi-week function, and viability of these cells types in culture.

UV-patterning adds another tool for exploring and scaling the production of patterned hydrogels for organ-on-chip applications [66]. In this proof-of-concept work, we only explored a small subset of possible patterns, with the goal of validating the ability to elicit the characteristic anisotropic organization of cardiac tissue. Scaling the production of human heart chips for toxicity testing is of particular interest because of the high incidence of cardiotoxicity in clinical drug trials [67]. The potential use of UV-M gelatin substrates is, however, not restricted to cardiac muscle chips. The engineering of other highly polarized and anisotropic organ tissues, such as neural tissue and skeletal muscle, equally benefit from micropatterned substrates [68]. Topographically patterned surfaces can also be used to mimic tissue-tissue interfaces and evoke characteristic cellular behaviors at these boundaries such as altered cell adhesion, migration, proliferation and matrix deposition. This suggests that UV micropatterning has high applicability to organ chips by probing the dynamic interplay of mechanical forces and different cell types involved in forming healthy and diseased tissue interfaces [68–70]. Further, though not explored in this study, we believe that it would be possible to UV-pattern other hydrogels commonly used in cell culture and tissue

engineering, such as alginate or PEG, as long as controlled film height, homogeneous absorption of riboflavin-5'phosphate, and full, non-destructive drying can be achieved to enable the etching by the laser.

The UV-patterning method allows separating the process of substrate fabrication and substrate patterning in both space and time. Such modular fabrication has a great potential to further increase throughput and flexibility because it enables batch processing, which reduces the relative cost of time-intensive start-up and calibration steps. Specifically, large quantities of unpatterned gelatin films could be prepared using dedicated injection molding or spin-coating setups [71–73]. Once dried, these samples can then be stored for "on-demand" patterning, eliminating the multi-day delay between pattern design and sample fabrication typical for micromolding and the associated photolithography steps [5, 32, 73]. Also, batch fabrication is facilitated because multiple samples can be laser-patterned automatically in one session, only limited by the availability of plain gelatin films which, as mentioned before, can be cast in large numbers any time prior without having to decide about the patter in advance. Importantly, the UV-patterning step could be further scaled and standardized for batch processing by using a motorized stage that moves a set of samples through the active laser zone, similar to an assembly line. In contrast, the number of micromolded samples made per day is inherently constraint by the fact that micromolding requires careful manual one-by-one alignment of the stamps and is further limited to the number of available stamps, which can only be made in advance if the desired pattern is already known.

In this proof-of-concept study, we demonstrate the suitability of UV-laser mediated micropatterning of gelatin films for the fast, flexible, and large-scale production of organ-on-chip substrates. Future work will focus on the use of other patterns and cell types, including astroglia and neurons, and skeletal muscle, to be used in brain chips and musculoskeletal chips, respectively. Further, using the measures discussed above, the process of gelatin film casting and UV patterning will be improved in efficiency to be able to manufacture hundreds, up from the current dozens, of identical substrates at a time. These high numbers can be realized by the fast and flexible UV-patterning method presented in this study.

Supplementary Material

Refer to Web version on PubMed Central for supplementary material.

Acknowledgments

We thank the Wyss Institute of Biologically Inspired Engineering and John A. Paulson School of Engineering at Harvard University for their support for this project. We also thank the Harvard Center for Nanoscale Systems for use of cleanroom facilities and atomic force microscope. We thank Brian Fountaine and Michael Rosnach, artists in residence, for their work on the graphic designs and photography in the figures of this manuscript. We thank Dr. Francesco Pasqualini for assistance with the orientational order parameter and sarcomeric packing density software developed in our laboratory. This work was funded by the United States Army, Defense Advanced Research Projects Agency Microphysiological Systems program, and the National Institutes of Health Grant (4UH3TR000522-03), National Science Foundation Materials Research Science and Engineering Center (MRSEC) grant DMR-1420570, and the Harvard John A. Paulson School of Engineering and Applied Sciences.

References

1. Parker KK, Ingber DE. Extracellular matrix, mechanotransduction and structural hierarchies in heart tissue engineering. Philosophical Transactions of the Royal Society B: Biological Sciences. 2007; 362(1484):1267–1279.
2. Capulli AK, et al. Fibrous scaffolds for building hearts and heart parts. Advanced Drug Delivery Reviews. 2016; 96:83–102. [PubMed: 26656602]
3. Gregorio CC, Antin PB. To the heart of myofibril assembly. Trends in Cell Biology. 2000; 10(9): 355–362. [PubMed: 10932092]
4. Bray M-A, Geisse NA, Parker KK. Multidimensional Detection and Analysis of Ca(2+) Sparks in Cardiac Myocytes. Biophysical Journal. 2007; 92(12):4433–4443. [PubMed: 17369419]
5. McCain ML, et al. Micromolded gelatin hydrogels for extended culture of engineered cardiac tissues. Biomaterials. 2014; 35(21):5462–71. [PubMed: 24731714]
6. Bhana B, et al. Influence of substrate stiffness on the phenotype of heart cells. Biotechnology and Bioengineering. 2010; 105(6):1148–1160. [PubMed: 20014437]
7. McCain ML, et al. Recapitulating maladaptive, multiscale remodeling of failing myocardium on a chip. Proceedings of the National Academy of Sciences. 2013; 110(24):9770–9775.
8. Wang N, Butler JP, Ingber DE. Mechanotransduction Across the Cell Surface and Through the Cytoskeleton. Science. 1993; 260(5111):1124–1127. [PubMed: 7684161]
9. Kujala VJ, et al. Laminar ventricular myocardium on a microelectrode array-based chip. Journal of Materials Chemistry B. 2016; 4(20):3534–3543.
10. Alford PW, et al. Vascular smooth muscle contractility depends on cell shape. Integr Biol (Camb). 2011; 3(11):1063–70. [PubMed: 21993765]
11. Feinberg AW, et al. Controlling the contractile strength of engineered cardiac muscle by hierarchal tissue architecture. Biomaterials. 2012; 33(23):5732–41. [PubMed: 22594976]
12. Rodriguez ML, et al. Measuring the Contractile Forces of Human Induced Pluripotent Stem Cell-Derived Cardiomyocytes With Arrays of Microposts. Journal of Biomechanical Engineering. 2014; 136(5):0510051–05100510.
13. Sheehy SP, et al. Toward improved myocardial maturity in an organ-on-chip platform with immature cardiac myocytes. Experimental Biology and Medicine. 2017 1535370217701006.
14. Pasqualini Francesco S, , et al. Structural Phenotyping of Stem Cell-Derived Cardiomyocytes. Stem Cell Reports. 2015; 4(3):340–347. [PubMed: 25733020]
15. Zhang D, et al. Tissue-engineered cardiac patch for advanced functional maturation of human ESC-derived cardiomyocytes. Biomaterials. 2013; 34
16. Alford PW, et al. Biohybrid thin films for measuring contractility in engineered cardiovascular muscle. Biomaterials. 2010; 31(13):3613–21. [PubMed: 20149449]
17. Feinberg AW, et al. Muscular thin films for building actuators and powering devices. Science. 2007; 317(5843):1366–70. [PubMed: 17823347]
18. Bhatia SN, Ingber DE. Microfluidic organs-on-chips. Nat Biotech. 2014; 32(8):760–772.
19. Capulli AK, et al. Approaching the in vitro clinical trial: engineering organs on chips. Lab on a Chip. 2014; 14(17):3181–3186. [PubMed: 24828385]
20. Wang G, et al. Modeling the mitochondrial cardiomyopathy of Barth syndrome with induced pluripotent stem cell and heart-on-chip technologies. Nat Med. 2014; 20(6):616–623. [PubMed: 24813252]
21. Lind JU, et al. Instrumented cardiac microphysiological devices via multimaterial three-dimensional printing. Nat Mater. 2016 **advance online publication**.
22. Huh D, et al. Microfabrication of human organs-on-chips. Nat. Protocols. 2013; 8(11):2135–2157. [PubMed: 24113786]
23. Zhang YS, et al. Multisensor-integrated organs-on-chips platform for automated and continual in situ monitoring of organoid behaviors. Proceedings of the National Academy of Sciences. 2017; 114(12):E2293–E2302.
24. Birket MJ, et al. Expansion and patterning of cardiovascular progenitors derived from human pluripotent stem cells. Nat Biotech. 2015; 33(9):970–979.

25. Grosberg A, et al. Ensembles of engineered cardiac tissues for physiological and pharmacological study: heart on a chip. Lab Chip. 2011; 11(24):4165–73. [PubMed: 22072288]
26. Radisic M, et al. Functional assembly of engineered myocardium by electrical stimulation of cardiac myocytes cultured on scaffolds. Proceedings of the National Academy of Sciences. 2004; 101(52):18129–18134.
27. Khetan S, Burdick JA. Patterning hydrogels in three dimensions towards controlling cellular interactions. Soft Matter. 2011; 7(3):830–838.
28. Hu Y, You J-O, Aizenberg J. Micropatterned Hydrogel Surface with High-Aspect-Ratio Features for Cell Guidance and Tissue Growth. ACS Applied Materials & Interfaces. 2016; 8(34):21939–21945. [PubMed: 27089518]
29. Agarwal A, et al. Micropatterning Alginate Substrates for in vitro Cardiovascular Muscle on a Chip. Adv Funct Mater. 2013; 23(30):3738–3746. [PubMed: 26213529]
30. Sarig-Nadir O, et al. Laser Photoablation of Guidance Microchannels into Hydrogels Directs Cell Growth in Three Dimensions. Biophysical Journal. 2009; 96(11):4743–4752. [PubMed: 19486697]
31. Agarwal A, et al. Microfluidic heart on a chip for higher throughput pharmacological studies. Lab Chip. 2013; 13(18):3599–608. [PubMed: 23807141]
32. Whitesides GM, et al. Soft Lithography in Biology and Biochemistry. Annual Review of Biomedical Engineering. 2001; 3(1):335–373.
33. Beaulieu I, Geissler M, Mauzeroll J. Oxygen Plasma Treatment of Polystyrene and Zeonor: Substrates for Adhesion of Patterned Cells. Langmuir. 2009; 25(12):7169–7176. [PubMed: 19505169]
34. Sader JE, Chon JWM, Mulvaney P. Calibration of rectangular atomic force microscope cantilevers. Review of Scientific Instruments. 1999; 70(10):3967–3969.
35. Johnson KL, Kendall K, Roberts AD. Surface Energy and the Contact of Elastic Solids. Proceedings of the Royal Society of London. A. Mathematical and Physical Sciences. 1971; 324(1558):301–313.
36. Sheehy Sean P, , et al. Quality Metrics for Stem Cell-Derived Cardiac Myocytes. Stem Cell Reports. 2014; 2(3):282–294. [PubMed: 24672752]
37. Volfson D, et al. Biomechanical ordering of dense cell populations. Proceedings of the National Academy of Sciences. 2008; 105(40):15346–15351.
38. Kuczyński W, Żywucki B, Małecki J. Determination of Orientational Order Parameter in Various Liquid-Crystalline Phases. Molecular Crystals and Liquid Crystals. 2002; 381(1):1–19.
39. Drew NK, et al. Metrics for Assessing Cytoskeletal Orientational Correlations and Consistency. PLOS Computational Biology. 2015; 11(4):e1004190. [PubMed: 25849553]
40. Schneider CA, Rasband WS, Eliceiri KW. NIH Image to ImageJ: 25 years of image analysis. Nat Meth. 2012; 9(7):671–675.
41. Grosberg A, et al. Muscle on a chip: in vitro contractility assays for smooth and striated muscle. J Pharmacol Toxicol Methods. 2012; 65(3):126–35. [PubMed: 22521339]
42. Czerner M, et al. Determination of Elastic Modulus of Gelatin Gels by Indentation Experiments. Procedia Materials Science. 2015; 8:287–296.
43. Kurokawa YK, George SC. Tissue engineering the cardiac microenvironment: Multicellular microphysiological systems for drug screening. Advanced Drug Delivery Reviews. 2016; 96:225–233. [PubMed: 26212156]
44. Zhang YS, et al. Bioprinting 3D Microfibrous Scaffolds for Engineering Endothelialized Myocardium and Heart-on-a-Chip. Biomaterials.
45. Wollensak G, Spoerl E, Seiler T. Riboflavin/ultraviolet-a–induced collagen crosslinking for the treatment of keratoconus. American Journal of Ophthalmology. 2003; 135(5):620–627. [PubMed: 12719068]
46. McCall AS, et al. Mechanisms of Corneal Tissue Cross-linking in Response to Treatment with Topical Riboflavin and Long-Wavelength Ultraviolet Radiation (UVA). Investigative Ophthalmology & Visual Science. 2010; 51(1):129–138. [PubMed: 19643975]

47. Zhang Y, et al. Analysis of the effective dose of ultraviolet light in corneal cross-linking. International Journal of Ophthalmology. 2016; 9(8):1089–1093. [PubMed: 27588260]
48. Kamaev P, et al. Photochemical Kinetics of Corneal Cross-Linking with RiboflavinKinetics of Corneal Cross-Linking. Investigative Ophthalmology & Visual Science. 2012; 53(4):2360–2367. [PubMed: 22427580]
49. Diaz-Quijada GA, et al. Surface modification of thermoplastics-towards the plastic biochip for high throughput screening devices. Lab on a Chip. 2007; 7(7):856–862. [PubMed: 17594004]
50. Sultanova NG, Kasarova SN, Nikolov ID. Characterization of optical properties of optical polymers. Optical and Quantum Electronics. 2013; 45(3):221–232.
51. van Midwoud PM, et al. Comparison of Biocompatibility and Adsorption Properties of Different Plastics for Advanced Microfluidic Cell and Tissue Culture Models. Analytical Chemistry. 2012; 84(9):3938–3944. [PubMed: 22444457]
52. Gazoti Debessa CR, Mesiano Maifrino LB, Rodrigues de Souza R. Age related changes of the collagen network of the human heart. Mechanisms of Ageing and Development. 2001; 122(10): 1049–1058. [PubMed: 11389923]
53. Bettadapur A, et al. Prolonged Culture of Aligned Skeletal Myotubes on Micromolded Gelatin Hydrogels. Scientific Reports. 2016; 6:28855. [PubMed: 27350122]
54. Rizzieri R, et al. Superficial Wrinkles in Stretched, Drying Gelatin Films. Langmuir. 2006; 22(8): 3622–3626. [PubMed: 16584235]
55. Caldorera-Moore M, et al. Swelling behavior of nanoscale, shape- and size-specific, hydrogel particles fabricated using imprint lithography. Soft Matter. 2011; 7(6):2879–2887.
56. Berry MF, et al. Mesenchymal stem cell injection after myocardial infarction improves myocardial compliance. American Journal of Physiology - Heart and Circulatory Physiology. 2006; 290(6):H2196–H2203. [PubMed: 16473959]
57. Dabiri GA, et al. Myofibrillogenesis visualized in living embryonic cardiomyocytes. Proceedings of the National Academy of Sciences. 1997; 94(17):9493–9498.
58. Bray MA, et al. Nuclear morphology and deformation in engineered cardiac myocytes and tissues. Biomaterials. 2010; 31(19):5143–50. [PubMed: 20382423]
59. Fu J, et al. Mechanical regulation of cell function with geometrically modulated elastomeric substrates. Nat Meth. 2010; 7(9):733–736.
60. Lee J. Methods in Cell Biology. Academic Press; 2007. The Use of Gelatin Substrates for Traction Force Microscopy in Rapidly Moving Cells; 295–312.
61. Aratyn-Schaus Y, et al. Coupling primary and stem cell–derived cardiomyocytes in an in vitro model of cardiac cell therapy. The Journal of Cell Biology. 2016
62. Nesmith AP, et al. A human in vitro model of Duchenne muscular dystrophy muscle formation and contractility. The Journal of Cell Biology. 2016
63. Eric SH, et al. Long-term vascular contractility assay using genipin-modified muscular thin films. Biofabrication. 2014; 6(4):045005. [PubMed: 25245868]
64. Yanagawa F, Sugiura S, Kanamori T. Hydrogel microfabrication technology toward three dimensional tissue engineering. Regenerative Therapy. 2016; 3:45–57.
65. Discher DE, Janmey P, Wang Y-l. Tissue Cells Feel and Respond to the Stiffness of Their Substrate. Science. 2005; 310(5751):1139–1143. [PubMed: 16293750]
66. Verhulsel M, et al. A review of microfabrication and hydrogel engineering for microorgans on chips. Biomaterials. 2014; 35(6):1816–1832. [PubMed: 24314552]
67. Arrowsmith J, Miller P. Trial Watch: Phase II and Phase III attrition rates 2011–2012. Nat Rev Drug Discov. 2013; 12(8):569–569. [PubMed: 23903212]
68. Nikkhah M, et al. Engineering microscale topographies to control the cell–substrate interface. Biomaterials. 2012; 33(21):5230–5246. [PubMed: 22521491]
69. Hamilton DW, Wong KS, Brunette DM. Microfabricated Discontinuous-Edge Surface Topographies Influence Osteoblast Adhesion, Migration, Cytoskeletal Organization, and Proliferation and Enhance Matrix and Mineral Deposition In Vitro. Calcified Tissue International. 2006; 78(5):314–325. [PubMed: 16604286]

70. Ning D, et al. Mechanical and Morphological Analysis of Cancer Cells on Nanostructured Substrates. Langmuir. 2016; 32(11):2718–2723. [PubMed: 26920124]

71. Wilson ME, et al. Fabrication of circular microfluidic channels by combining mechanical micromilling and soft lithography. Lab on a Chip. 2011; 11(8):1550–1555. [PubMed: 21399830]

72. Gitlin L, Schulze P, Belder D. Rapid replication of master structures by double casting with PDMS. Lab on a Chip. 2009; 9(20):3000–3002. [PubMed: 19789756]

73. Scott B, et al. Soft lithography and microfabrication. Physics World. 1998; 11(5):31.

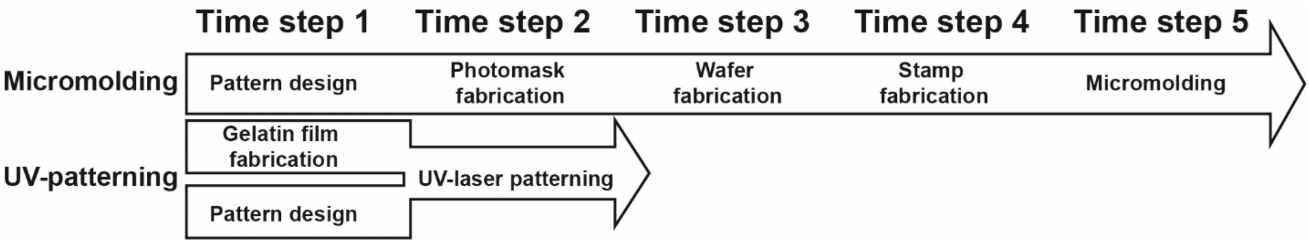

Fig. 1. Workflow and timeline of UV-patterning approach compared to traditional micromolding

This schematic overview shows the steps required for designing and fabricating patterned gelatin substrates start-to-finish using traditional micromolding (top) or UV-patterning (bottom) fabrication. Micromolding involves a 5-time step sequence of interdependent steps, compared to a 2-time step process using UV-patterning. This 60% faster work flow is possible because UV-patterning eliminates the photolithography steps enabling separation and parallelization of work steps, such as pattern design and gelatin film fabrication.

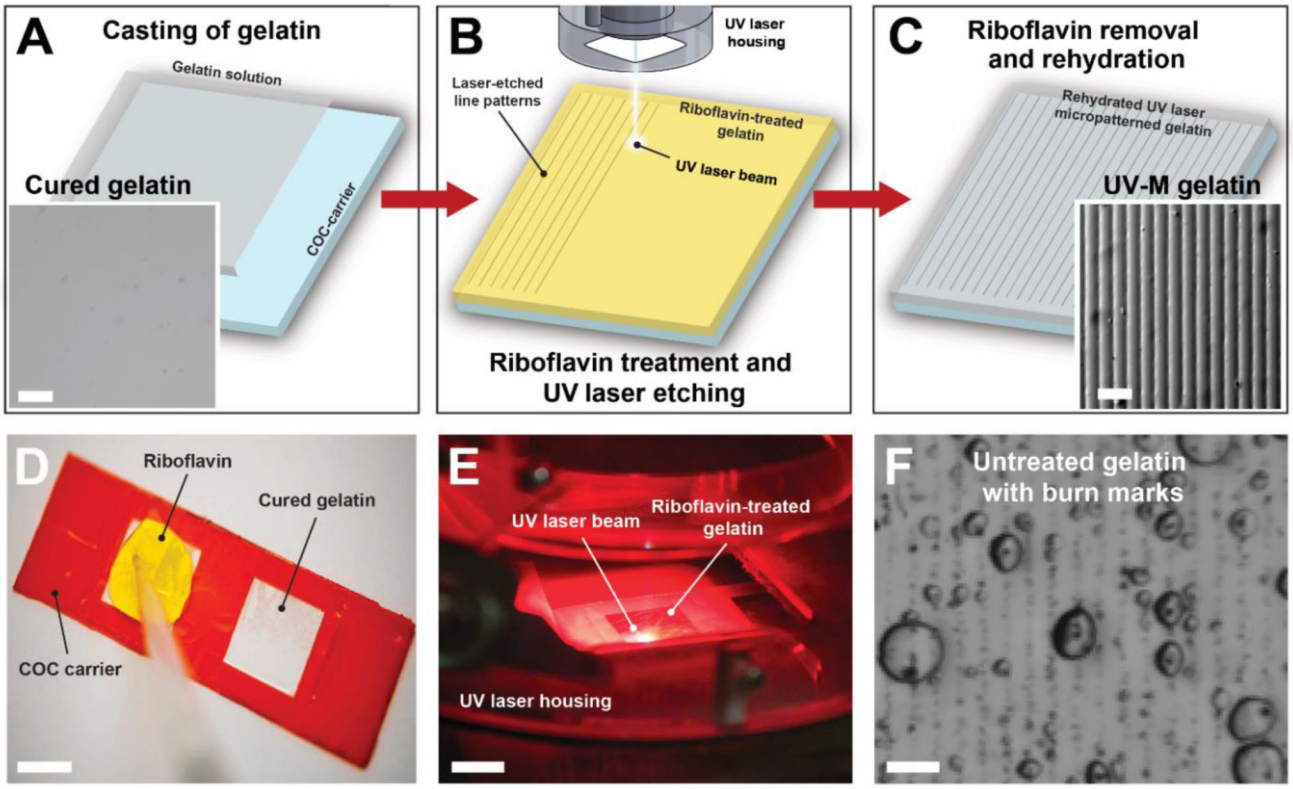

Fig. 2. Fabrication of UV laser micropatterned hydrogels for tissue engineering

(A) Gelatin solution (gray) containing the cross-linking agent microbial transglutaminase is cast onto a COC carrier slide (blue) and allowed to cure for 12 hours. Inset: Stereomicroscope image of cured gelatin hydrogel surface. (B) Gelatin hydrogels are treated with aqueous riboflavin-5'phosphate solution (yellow), dried, and subsequently micropatterned with a 15-μm-wide UV laser beam (355 nm wavelength). (C) Hydrated and rinsed gelatin (gray) with UV laser micropatterned lines. Inset: Stereomicroscope image of micropatterned gelatin surface. Scale bars are 50 μm. (D) Addition of 0.05% riboflavin-5'phosphate to the gelatin surface. (E) UV laser etching of gelatin surface. Scale bar is 1 cm. (F) Untreated gelatin hydrogels cannot be effectively micropatterned with the UV laser engraver and instead exhibit burn marks and bubbles. Scale bar is 50 μm.

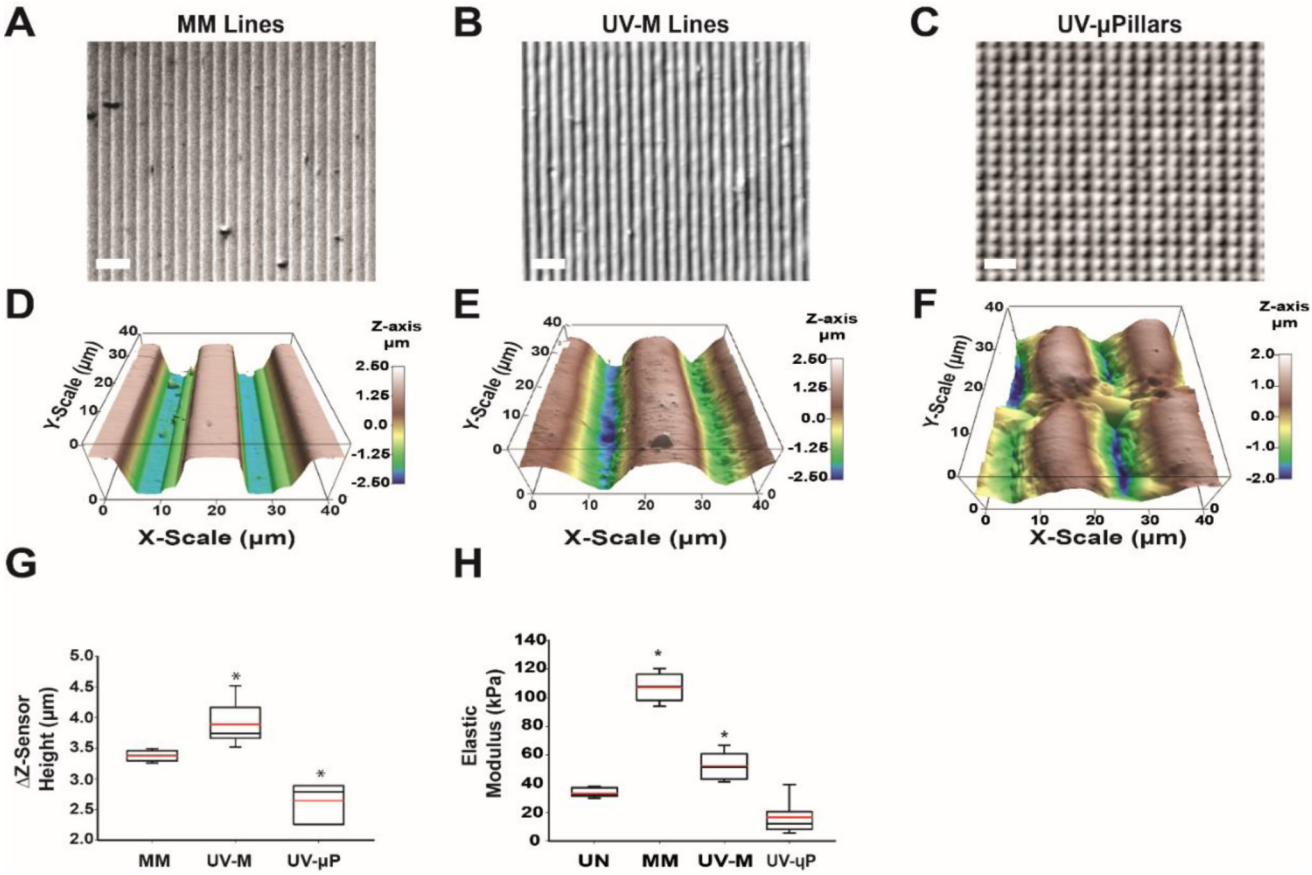

Fig. 3. Micromechanics of molded and UV laser micropatterned hydrogels

(A-C) Brightfield images of (A) micromolded (MM) gelatin lines, (B) UV micropatterned (UV-M) lines, and (C) UV micropatterned square pillars (UV-µP). Scale is 50 µm. (D-F) Contact-mode AFM topography images in 3D for (D) MM gelatin, (E) UV-M gelatin, and (F) UV-µP gelatin in liquid over an area of 40 μm^2 with a Z-sensor height range of 5 µm. (G) Differences in maximum and minimum Z-sensor heights (ΔZ-sensor height) for MM, UV-M, and UV-µP gelatin (n = 6–13, 2–4 samples each). *P<0.05 compared to MM gelatin by Kruskal-Wallis One Way ANOVA (H) Box and whisker plot of elastic moduli of UN, MM, UV-M, and UV-µP where a minimum of n = 75 FDCs were used for each Z-level of the pattern. The red line represents the mean, black center line represents the median, and error bars represent the 5^{th} and 95^{th} percentile. *P<0.05 compared to UN gelatin by Kruskal-Wallis One Way ANOVA

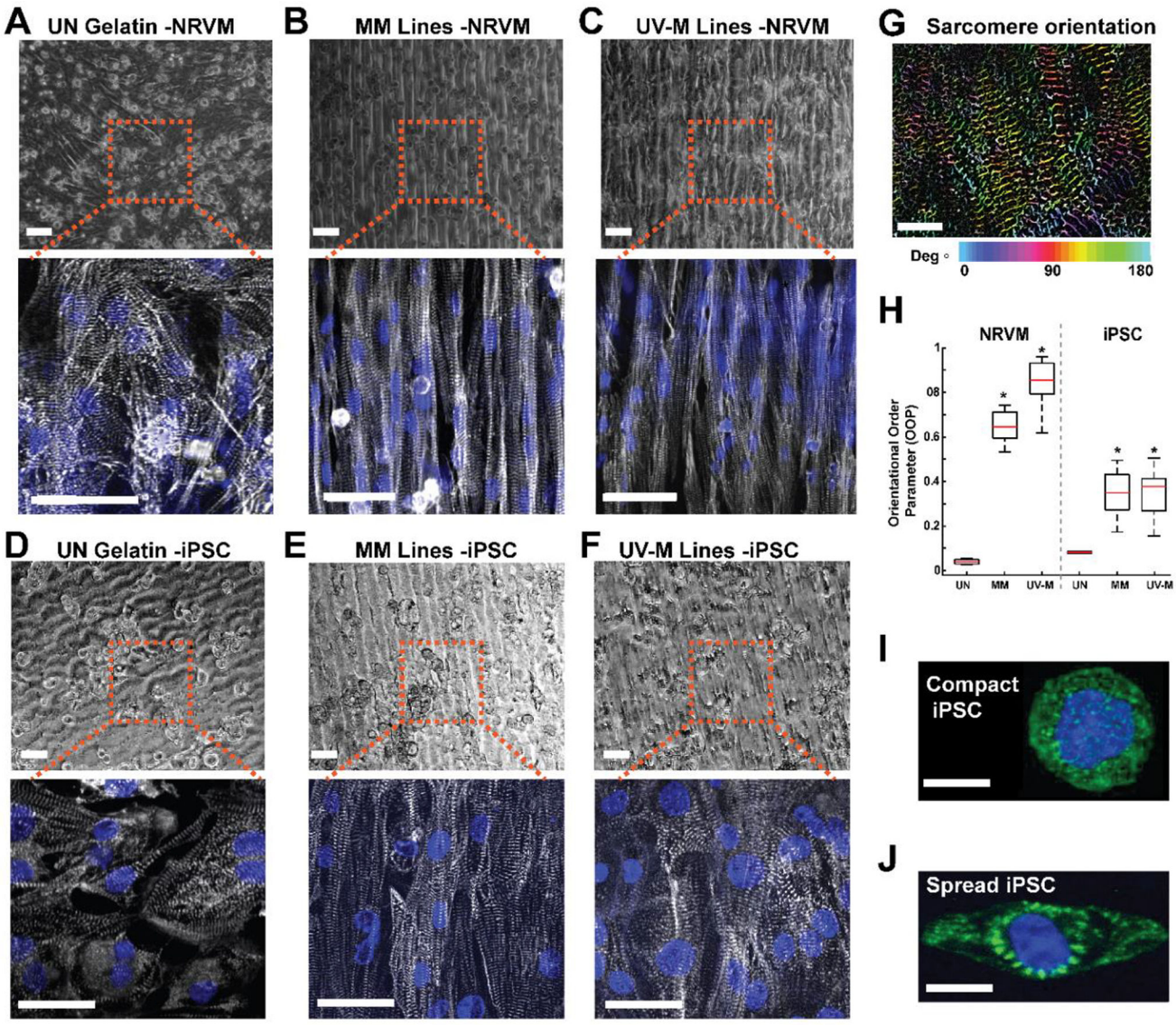

Fig. 4. Cardiac tissue engineering of neonatal rat ventricular myocytes and human iPSCs with UV laser micropatterning

(A-C) NRVMs seeded on (A) unpatterned (UN) gelatin, (B) MM gelatin, and (C) UV-M gelatin lines after 5 days in culture. Top: Bright field image. Scale is 50 μm. Bottom: Immunohistochemistry. Blue = chromatin, gray = α-actinin. Scale is 25 μm. (D-F) Human iPSCs seeded on (D) unpatterned (UN) gelatin, (E) MM gelatin, and (F) UV-M gelatin lines. Top: Bright field image. Scale is 40 μm. Bottom: Immunohistochemistry. Blue = chromatin, gray = α-actinin. Scale is 15 μm. (G) Example of intermediate OOP analysis step. Sarcomeres are detected through filtering and thresholding, and their relative orientation angles are computed using the image structure tensor. The orientation angle of each sarcomere is indicated through a color-code. Scale is 5 μm. (H) Box plot of orientational order parameter (OOP) of sarcomeric α-actinin in NRVM tissues engineered on UN (n = 3 slides, 8 images), MM (n= 4 slides, 24 images), and UV-M gels (n= 4 slides, 44 images), and in human iPSC tissues engineered on UN (n = 1 slide, 2 images), MM (n= 1 slide, 14

images), and UV-M gels (n= 2 slides, 20 images). The red line represents the mean, black center line represents the median, and bars represent 5^{th} and 95^{th} percentiles. *P < 0.05 vs. UN gelatin by Kruskal-Wallis one way ANOVA and Dunn's Test. (I) Immunostained single compact iPSC on a UV μ-pillar island. Scale bar is 10 μm. (J) Immunostained single iPSC spread beyond the UV μ-pillar island. Green: α-actinin, blue: chromatin. Scale bar is 10 μm.

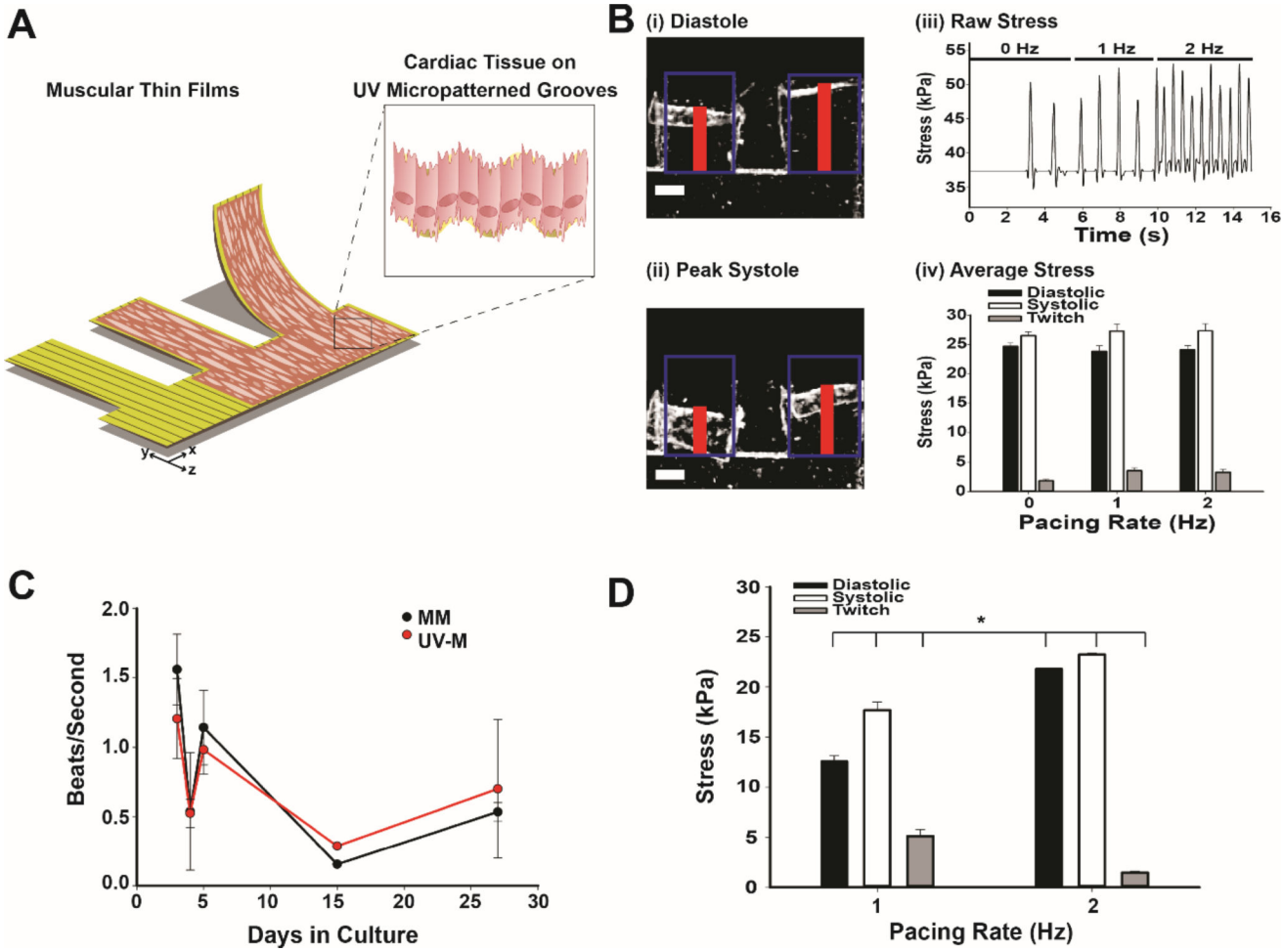

Fig. 5. Heart-on-a-chip applications of UV laser micropatterning

(A) Schematic of MTFs using UV laser micropatterning. (B) UV-M engineered MTFs: (i) Stereoscope brightfield images of engineered NRVM cardiac muscular thin films in diastole and systole (ii) after 5 days in culture. Red line indicates height of MTF detected by tracking software. Blue boxes represent initial length. Scale bar is 0.5 mm. (iii) Raw contractile stress traces at 0, 1, and 2 Hz pacing frequencies for the same representative MTF. (iv) Contractile stress of UV laser micropatterned muscular thin films (n = 9–13 films, 5–6 heart chips). Bars represent the mean ± SEM for diastolic (black), systolic (white), and twitch stress (gray). (C) Beat rate of engineered MM (black) and UV-M (red) NRVM cardiac tissues in culture over a 27 day period in beats per second. (D) Contractile stress of UV-M muscular thin films after 27 days in culture (n = 2–3 films, 1 heart chip). Bars represent the mean ± SEM for diastolic (black), systolic (white), and twitch stress (gray). *P<0.05 compared to 1 Hz pacing by Student's T-Test.